Metallic porous electrodes enable efficient electrolysis of liquid CO_2 capture solutions

Zishuai Zhang,[1#] Eric W. Lees,[2#] Faezeh Habibzadeh,[1] Danielle A. Salvatore,[2] Shaoxuan Ren,[1] Grace Simpson,[2] Danika Wheeler[2] Alyssa Liu[1] and Curtis P. Berlinguette*[1,2,3,4]

[1]Department of Chemistry, The University of British Columbia, 2036 Main Mall, Vancouver, British Columbia, V6T 1Z1, Canada.

[2]Department of Chemical and Biological Engineering, The University of British Columbia, 2360 East Mall, Vancouver, British Columbia, V6T 1Z3, Canada.

[3]Stewart Blusson Quantum Matter Institute, The University of British Columbia, 2355 East Mall, Vancouver, British Columbia, V6T 1Z4, Canada.

[4]Canadian Institute for Advanced Research (CIFAR), 661 University Avenue, Toronto, M5G 1M1, Ontario, Canada.

[#] These authors contributed equally to this work

*Corresponding author: Curtis P. Berlinguette (cberling@chem.ubc.ca)

Abstract

We demonstrate here that a porous free-standing silver foam cathode in an electrolytic flow electrolyzer mediates efficient electrolysis of 3.0 M bicarbonate solutions into CO. These results have direct implications for carbon capture schemes where OH^- solutions react with CO_2 to form bicarbonate-rich solutions that need to be treated to recycle the sorbent and recover the CO_2. Our study shows a viable path for replacing the high-temperature thermal process currently used to recover CO_2 from these carbon capture solutions by using electricity to drive the conversion of bicarbonate into CO_2 and subsequently into CO. The use of free-standing porous silver electrodes was found to yield electrolysis performance parameters (e.g., a Faradaic efficiency for CO production, FE_{CO}, of 95% at 100 mA cm^2; <3% performance loss after 80 h operation) that are superior to results obtained in bicarbonate electrolyzers that utilize conventional carbon-based gas diffusion electrodes (GDEs) designed for gaseous CO_2 fed electrolyzers. This liquid-fed bicarbonate electrolyzer achieves high CO formation rates with the added benefit of not requiring an energy-intensive CO_2 regeneration step that would be necessary for the electrolysis of gaseous CO_2. These findings represent a potentially important step in closing the carbon cycle.

TOC figure

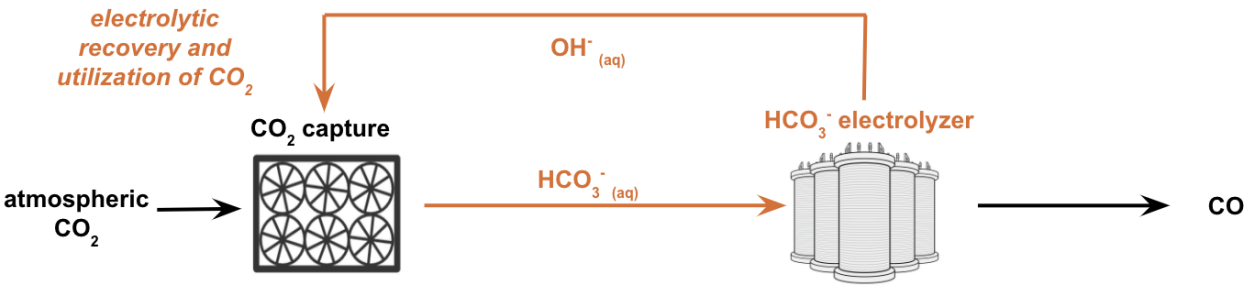
electrolytic recovery and utilization of CO_2
$OH^-_{(aq)}$
CO_2 capture
HCO_3^- electrolyzer
atmospheric CO_2
$HCO_3^-_{(aq)}$
CO

Introduction

In order to utilize CO_2 captured from the atmosphere or a point source, the captured CO_2 needs to be extracted from the sorbent in such a way that the sorbent can be recycled to capture additional CO_2. Schemes that rely on basic solutions such as KOH to capture CO_2 by forming carbonate (Eqs. 1 and 2) use a high temperature calcination step (>900 °C) to subsequently liberate CO_2 (which can then be stored or utilized) from the carbonate salt with the concomitant recovery of the OH^- sorbent (Eqs. 3 and 4, Figure 1).[1] This recovery process involving the thermal decomposition of $CaCO_3$ at 900 °C is expensive because it uses two preheat cyclones along with a calciner in succession that are both energy and capital intensive.[1] One promising option for using this CO_2 is to electrolytically convert it into chemicals or fuels of economic value (e.g., CO) using renewable electricity (Eq. 5, Figure 1).[2,3] While there have been many recent advances in electrolytic CO_2 reduction,[2,4–7] the electrolysis of CO_2 will likely require an energy-intensive CO_2 pressurization step prior to electrolysis in order to achieve meaningful reaction rates (Figure 1).[8] Purification of the gaseous CO_2 is also necessary to remove impurities (O_2,[9] NO_x,[9] SO_x,[10] NH_3,[11] HCl[12]) which reduce the efficiency of the electrolyzer.[9,10]

CO_2 capture:	$CO_{2\,(g)} + 2\ KOH_{(aq)} \rightleftharpoons K_2CO_{3\,(aq)} + H_2O_{\,(l)}$, ($pK_b$ 3.7)	Eq. 1
KOH regeneration:	$K_2CO_{3(aq)} + Ca(OH)_{2\,(s)} \rightleftharpoons CaCO_{3\,(s)} + 2\ KOH_{(aq)}$	Eq. 2
CO_2 recovery:	$CaCO_{3\,(s)} \rightleftharpoons CO_{2\,(g)} + CaO_{\,(s)}$	Eq. 3
Sorbent regeneration:	$CaO_{\,(s)} + H_2O_{\,(l)} \rightleftharpoons Ca(OH)_{2\,(s)}$	Eq. 4
CO_2 reduction reaction (CO_2RR):	$CO_{2\,(g)} + H_2O_{(l)} + 2e^- \rightleftharpoons CO_{(g)} + 2OH^-_{(aq)}$	Eq. 5

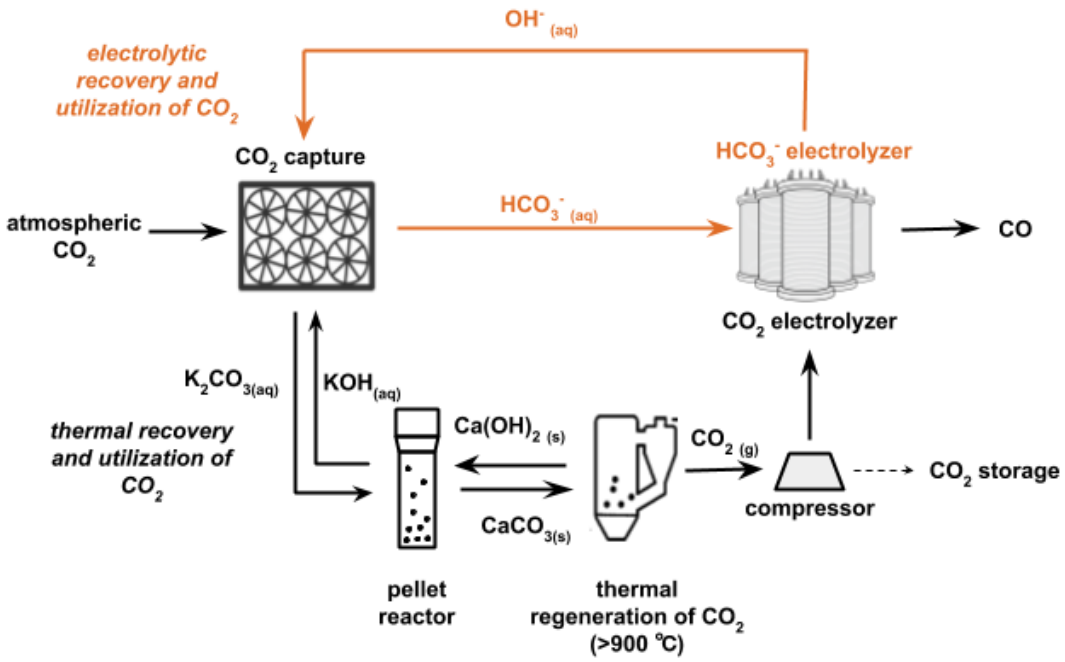

Figure 1. **Thermal CO_2 and sorbent recovery (black) and electrolytic CO_2 recovery (orange) processes that convert captured atmospheric CO_2 to CO.** For the direct air capture process, atmospheric $CO_{2(g)}$ is captured by hydroxide solutions and then regenerated from $CaCO_{3(s)}$ in a high temperature calcination step (>900 °C). The recovered CO_2 typically needs to be pressurized prior to electrolysis or storage (black). For the bicarbonate electrolysis process, carbon capture solution (HCO_3^-) is electrochemically converted to CO without the need for energy intensive calcination and pressurization steps (orange). The hydroxide byproduct can be recycled for use as a carbon capture solution in the bicarbonate electrolysis pathway.

Our program is therefore seeking methods that avoid the calcination and pressurizations steps by developing reactor architectures that utilize bicarbonate solutions obtained during the CO_2 capture process as the cathodic feedstock while regenerating the OH^- sorbent for subsequent carbon capture (Figure 1).[1,13–16] This proposed carbon capture and utilization scheme links CO_2 electrochemistry with upstream carbon capture without requiring high temperature or pressurization processes. A major technical challenge associated with this scheme is that bicarbonate cannot be directly electrochemically reduced at an industrial-relevant current density (≥ 200 mA cm^{-2}). Bicarbonate must first react with protons to form CO_2, which is the electrocatalytically active species that can be reduced to CO or other

carbon-containing products. The management of this acid-base chemistry (Eq. 6) in tandem with electrochemistry (Eq. 5) therefore requires the careful design of an electrolyzer before liquid bicarbonate feedstocks can be deemed suitable for electrolysis. It is for these reasons that we are seeking ways to have protons delivered from a membrane, such as a bipolar membrane (BPM), for reaction with bicarbonate to form electrocatalytically active CO_2 at the membrane-catalyst interface (Figure 2a).[15,17]

$$\textit{Conversion of bicarbonate:} \quad H^+_{(aq)} + HCO_3^-{}_{(aq)} \rightleftharpoons H_2O_{(l)} + CO_{2\,(g)} \qquad \text{Eq.6}$$

For electrolyzers that use a gaseous CO_2 feedstock, gas diffusion electrodes (GDEs) are designed to support an electrocatalyst layer while also managing the water content at the cathodic side of the membrane electrode assembly (MEA). Flooding of the MEA with water needs to be avoided because it decreases the performance of electrolyzers by hindering CO_2 access to the catalyst layer. Excess water also promotes the undesirable hydrogen evolution reaction (HER) to occur over the CO_2 reduction reaction (CO_2RR).[18] GDEs (i.e., carbon composite electrode) used for electrolysis of gaseous CO_2 typically consist of a three-layer structure containing: (i) a conductive, porous carbon cloth positioned against the cathodic flow plate; (ii) a conductive and hydrophobic microporous layer (MPL) of carbon black treated with polytetrafluoroethylene (PTFE); and (iii) a catalyst layer between the MPL and the membrane (Figure 2b). The hydrophobicity of the MPL serves to mitigate flooding, and the mitigated flooding helps reduce ohmic losses and increases the accessible active area of the catalyst layer.[19]

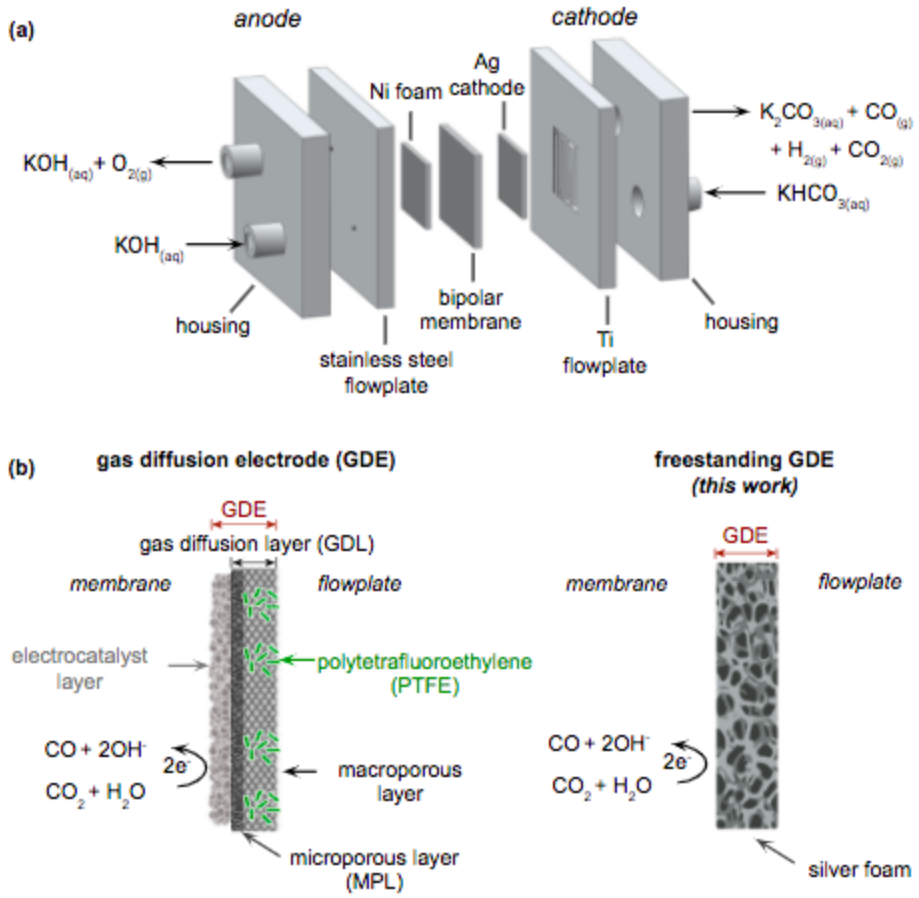

Figure 2. **The flow electrolyzer and free-standing silver foam electrode used in this work .** (a) Schematic depiction of the flow electrolyzer with bipolar membrane (BPM), silver cathodes (e.g., carbon composite and silver foam electrodes) and bicarbonate feedstock.(b) Schematic depictions of the conventional GDE cathode with a microporous layer (MPL) and polytetrafluoroethylene (PTFE) treatment, and the free-standing silver foam electrode. Bicarbonate ions are the reactants for *in-situ* CO_2 generation at the membrane-catalyst interface, and the produced CO_2 is subsequently reduced to CO (see Eqs. 5 and 6).

While these composite electrode designs are effective for the electrolysis of *gaseous* CO_2, they are not necessarily effective for the electrolysis of *liquid* feedstocks such as bicarbonate. Consider that commercial liquid-fed electrolyzer systems (e.g., water electrolyzers and chlor-alkali electrolyzers),[20,21] use free-standing electrodes and not the carbon composite electrodes as described above. Free-standing porous nickel (alloys), or steel electrodes coated with nickel, are capable of operating at lower overpotentials with longer lifetimes relative to carbon composite electrodes in alkaline water

electrolyzers.[22,23] Commercial chlor-alkali electrolyzers also use titanium-based and nickel-based free-standing electrodes.[21,24,25] Moreover, hydrophobic composite electrode inhibit the transport of solvated HCO_3^-, therefore adversely affecting the *in-situ* CO_2 generation (*i*-CO_2) at the membrane-electrode interface.[26] Replacing hydrophobic composite electrode with metallic porous electrodes is anticipated to facilitate the transport of solvated ions and improve the performance of the bicarbonate electrolyzer.[27]

These collective observations inspired us to test porous free-standing silver foam electrodes for liquid bicarbonate fed electrolysis. Not only these free-standing electrodes simplify the assembly of electrolyzers relative to conventional composite electrodes (which require a multi-step fabrication process), these metallic electrodes mediate remarkably effective bicarbonate electrolysis (e.g., a faradaic efficiency for CO production (FE_{CO}) of 95% at 100 mA cm^{-2} and 55% at 400 mA cm^{-2}) and incur a mere 3% loss in FE_{CO} over 80 h of sustained electrolysis at 65 mA cm^{-2}. These results are superior to that of our control bicarbonate electrolysis experiments with carbon composite electrodes (i.e., multilayer structure of a catalyst layer adjacent to a hydrophobic GDL as a support) that has demonstrated high performance in gaseous-fed CO_2 electrolyzers. We achieved these state-of-the-art results by systematically optimizing the pressure, temperature, and flow plate design of the bicarbonate electrolyzer. Moreover, we show that the catalytic activity of our metallic electrodes is not impaired by the majority of flue gas impurities which commonly form NO_3^-, SO_4^{2-}, SO_3^{2-}, NH_4^+, Cl^- in CO_2 capture solutions.[28] The bicarbonate electrolyzers reported herein achieve promising CO formation rates relative to state-of-art gaseous CO_2-fed electrolyzers (Table S1), providing an opportunity to close the current upstream carbon capture loop and to avoid the costly calcination and pressurization steps.

Results and Discussion

All electrolysis experiments were conducted in a two-electrode MEA electrolyzer (Figure 2a).[15,29] The MEA consisted of a fully hydrated Fumasep bipolar membrane (BPM) sandwiched between the anode (Ni foam) and the cathode (conventional GDEs or silver foam-based electrodes). The BPM was operated in reverse-bias mode, with the cation exchange layer facing the cathode.[17] A peristaltic pump delivered 1.0 M KOH to the anode at a constant flow rate of 40 ml min^{-1}. The 3.0 M $KHCO_3$ cathode electrolyte was delivered separately at a constant flow rate of 100 ml min^{-1}. The headspace of the cathode electrolyte reservoir was purged with N_2 at 160 sccm over the course of each experiment. Product gases and N_2 in the headspace of the cathode electrolyte reservoir were delivered to an in-line gas chromatograph (GC) with data analysis and peak integration completed in PeakSimple software. .

The bicarbonate electrolysis experiments were designed to test modifications of the cathodes: carbon composite electrode and silver foam electrode (Figure 2b). Silver was selected as the cathode of choice because it mediates effective conversion of CO_2 to CO.[30,31] The silver foam electrode (2 cm × 2 cm × 150 μm) were prepared by etching commercially available silver foam in dilute nitric acid (30% v/v HNO_3) for 10 seconds (Figure 2b).

Scanning electron microscopy (SEM) imaging of the etched surface of the silver foam contains a high number of cracks and holes (Figure S1). The X-ray diffraction (XRD) measurements of the foam electrode indicated signals at 38°, 44° and 64° corresponding to metallic silver (111), (200) and (220) facets, respectively (Figure S2). These signals are consistent with metallic silver (Ag^0) being the main constituent of the samples. The electrochemical surface areas (ECSA) of the silver electrocatalyst in the silver foam electrode, estimated from the double-layer capacitance (C_{dl}) measurements (Figure S3), were significantly higher than that of the carbon composite electrode. The etching process increased the ECSA of the silver foam electrode by ~1.2-fold. Beyond changes in ECSAs, the specific activity of the acid-etched silver foam electrode was also measured to be higher than the untreated foam. This effect

made be due to the rougher curved surfaces that have been reported to stabilize CO_2^- intermediates (i.e., a higher roughness factor; roughness factor = ECSA / geometric electrode area) (Figure S4).[32] The silver foam electrodes reported here were etched unless stated otherwise.

Effect of the silver foam cathode on bicarbonate electrolysis

Both the silver foam and carbon composite electrodes were tested in an electrolyzer under constant applied current densities of 100, 200 and 300 mA cm^{-2}. Control experiments were performed with a CeTech® woven carbon cloth support containing a layer of silver nanoparticles. This carbon support contains an MPL and PTFE common to gas-fed electrolyzers.[33,34] Electrolysis experiments using carbon composite electrodes at an applied current density of 100 mA cm^{-2} for 500 seconds yielded a FE_{CO} value of 33 ± 6%. This performance metric was exceeded by the silver foam electrode, which achieved a FE_{CO} value of 59 ± 6% at 100 mA cm^{-2}. This difference in FE_{CO} was maintained over a 100-300 mA cm^{-2} range (Figure 3). At 100 mA cm^{-2}, the cell voltage (V_{cell}) of the foam electrode (3.6 ± 0.1 V) was slightly higher than that of the carbon composite electrode (3.4 ± 0.1 V, Figure S5). The higher cell voltages obtained with the foam electrodes relative to the carbon composite electrodes despite porous metals being two orders-of-magnitude more conductive than carbon GDLs (i.e., ~10^5.S m^{-1} [35] *c.f.* ~10^3 S m^{-1})[36]. This difference in cell potentials may therefore be related to a relatively higher tortuosity compared to composite electrodes, the foams retain larger volumes of the electrolyte which consequently introduces a greater solution resistance. Moreover, the contact resistances between the MPL and the membrane is lower.[37] These factors are difficult to experimentally resolve in a dynamic electrolyzer environment. Nevertheless, there are several properties of silver foam electrodes that can be tuned to reduce voltage losses: thickness, pore size distribution, surface roughness, etc.

We operated an electrolyzer at 100 mA cm^{-2} and tracked the amount of CO and CO_2 exiting the electrolyzer by GC to evaluate the CO_2 utilization values for both electrodes. Experiments showed the silver foam electrode containing electrolyzer reached a CO_2 utilization value of ~40%, which is nearly double that of the composite electrode (Figure S6). We also measured liquid CO2RR products formed during the preceding experiments using ^{1}H NMR spectroscopy to confirm that all $FE_{formate}$ values were <1% (Figure S7).

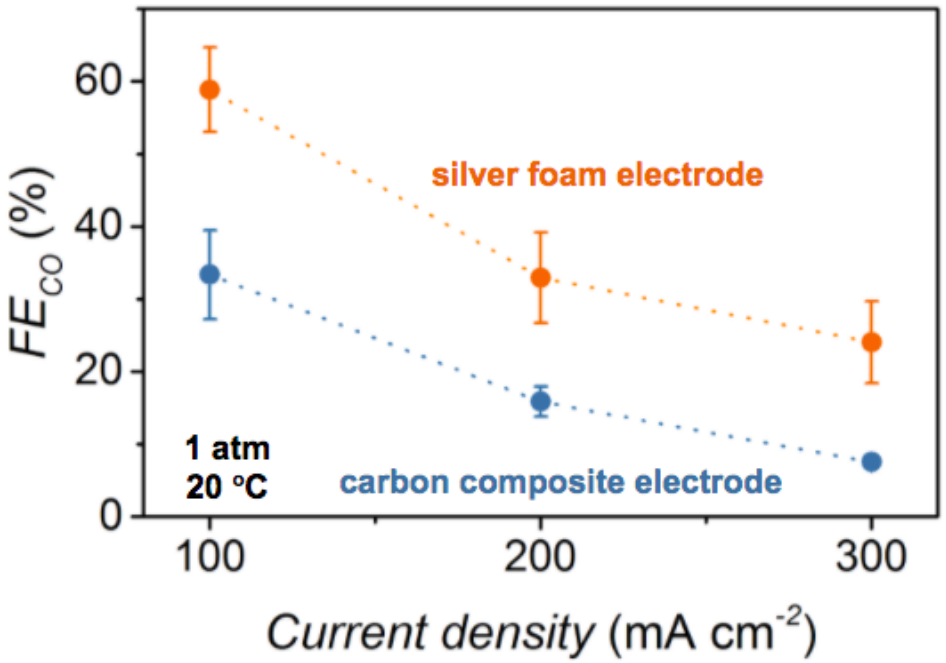

Figure 3. **The performance of the free-standing silver foam electrode.** FE_{CO} as a function of current density for the carbon composite electrode and silver foam electrode (geometrical surface area = 4 cm^2; bicarbonate solution at 20 °C; electrolyzer operated at 1 atm).

Effect of pressure and temperature on bicarbonate electrolysis

We conjectured that the CO formation rates from our bicarbonate electrolyzer could be improved by performing electrolysis at elevated temperatures and pressures. At higher pressures, the solubility of CO_2 in aqueous electrolyte increases,[38] which results in more CO_2 available for reaction at the electrolyte–electrocatalyst interface. We tested this hypothesis by constructing a pressurized bicarbonate electrolyzer test station (Figure S8; see Supporting Information for details) and applying constant current densities to our electrolyzer fitted with foam electrodes (Figure 4a**)**. Our results show that increasing the inlet pressure of the electrolyzer from 1-4 atm increased the FE_{CO} from 55% to 95% at a current density of 100 mA cm^{-2}. This result sets the benchmark for electrolytic CO formation from a CO2RR electrolyzer that uses a liquid feedstock (Table S1). Moreover, at these elevated pressures we observed a less pronounced decrease in FE_{CO} relative to ambient conditions as the current density was increased from 100 to 400 mA cm^{-2} (i.e., the FE_{CO} at 400 mA cm^{-2} remained above 55% for an inlet pressure of 4 atm, but decreased to 23% at 1 atm). These observations support the notion that increasing the electrolyzer pressure increases the kinetic supply of CO_2 to the electrocatalyst, and consequently, the rate of CO formation.

We also observed that the efficiency of bicarbonate electrolysis could also be improved by increasing the temperature of the electrolyte to 70 ^{o}C (Figure 4b). Using the foam electrodes, an electrolyte temperature at the electrolyzer inlet of 70 °C yielded a FE_{CO} of 78 at 100 mA cm^{-2} with a corresponding voltage of 3.5 V (*c.f.* FE_{CO} of 59 at 20 ^{o}C). Temperature can improve electrolyzer performance (i.e., improved FE_{CO}) in a number of ways and they are difficult to experimentally resolve in a dynamic electrolyzer environment. Higher temperatures increase CO_2 generation by increasing bicarbonate dissociation kinetics (Eq. 7),[39] and shifting the equilibrium towards CO_2 (Eq. 6, ΔH = 11.77 kJ mol^{-1}) (Figure S9). These reactions also increase the pH, thereby suppressing HER (Figure S10).[40] This observation is supported by the GC measurements. Higher temperatures would yield faster mass

transfer kinetics for HCO_3^- and CO_2, which would also be expected to enhance the rate of bicarbonate electrolysis.[41]

Bicarbonate dissociate: $HCO_3^- \leftrightharpoons OH^- + CO_2$ Eq.7

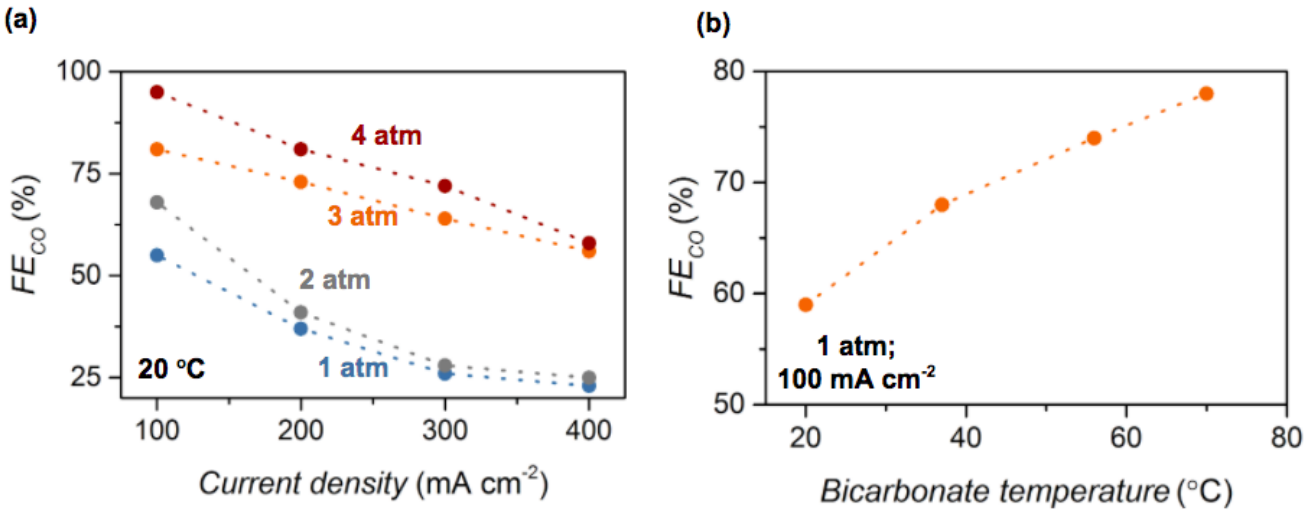

Figure 4. **The impact of operation conditions (pressure and temperature) on the bicarbonate electrolysis performance.** (a) FE_{CO} values as a function of pressure at different current densities. The pressure of the liquid feedstock was measured at the inlet of the electrolyzer (b) FE_{CO} values as a function of bicarbonate temperature (20, 37, 56 and 70 °C, measured at the inlet of the electrolyzer) at 100 mA cm^{-2}. The temperature of the bicarbonate solution was measured when the solution entered the cathodic flowplate. All tests were performed with the silver foam electrode.

Effect of convective mass transfer and flow plate design on bicarbonate electrolysis

We then sought to investigate the effect of convective fluid flow in the cathode compartment on the FE_{CO}. We first increased the convective mass transport of HCO_3^- by increasing the flow rate from 30 to 100 mL min^{-1} (Figure S11). This procedure led to an increase in *i*-CO_2, and, in turn, the selectivity (FE_{CO}).[26] The cell voltage did not change over this tested flow rate range.[42] Based on this result, we sought to further improve convective mass transfer in the

cathode compartment using different flow pattern geometries (interdigitated, serpentine, and parallel; Figure 5a). These flow plates were 3D printed using an acrylonitrile butadiene styrene (ABS) plastic, coated with silver paint to improve conductivity (Figure S12),[43] and tested in the electrolyzer with the foam electrode (Figure 5b). The electrolyzer with the interdigitated flow pattern exhibited the highest FE_{CO} values (69 ± 4% FE_{CO} at 100 mA cm^{-2}) of the flow plates tested, without any additional voltage or pressure drop penalty (Figures 5b, S13, S14). Given that mass transfer occurs primarily by convection for the interdigitated flow plate (diffusion dominates parallel and serpentine flow patterns),[44] this result is consistent with convective mass transfer being positively correlated to FE_{CO}.

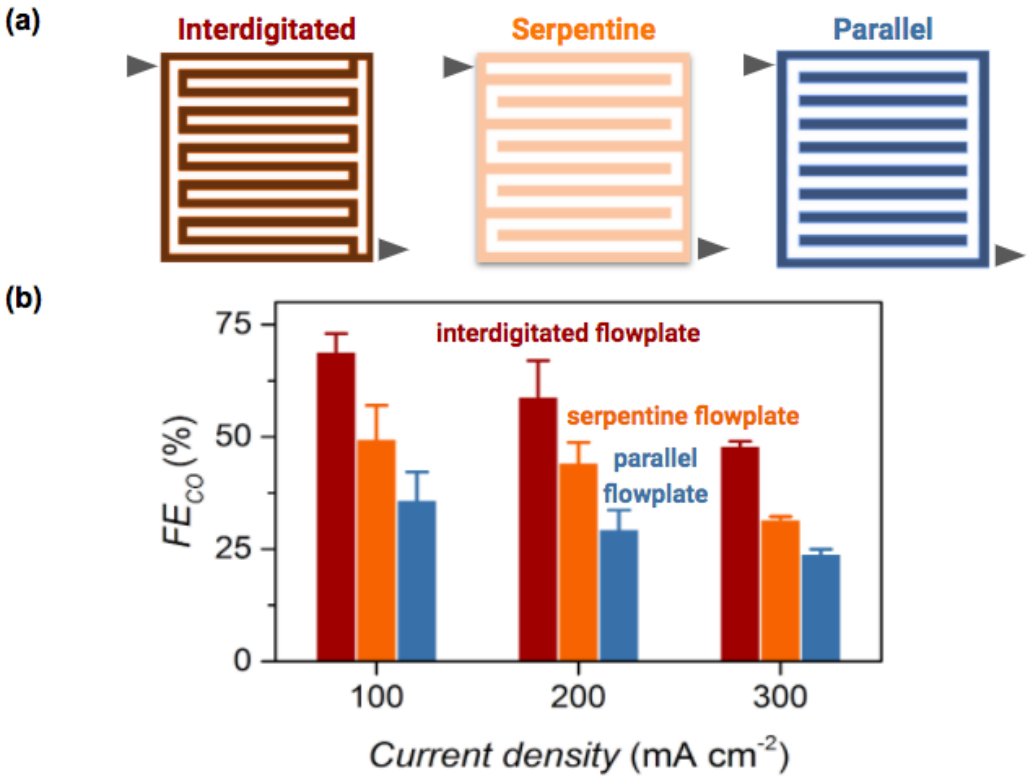

***Figure 5*. The impact of flowplates on the bicarbonate electrolyzer performance.** (a) Render of interdigitated, serpentine and parallel cathodic flow plate patterns. (b) FE_{CO} as a function of current density for interdigitated, serpentine, and parallel flow plates tested in the bicarbonate electrolyzer with silver foam electrodes.

Stability and the effects of flue gas impurities on bicarbonate electrolysis

Stability studies were performed by electrolysing 3.0 M bicarbonate over 80 hours at an applied current density of 65 mA cm^{-2} using an electrolyzer containing silver foam based electrodes or carbon composite electrodes (Figure S15). (We recorded data at 65 mA cm^{-2} instead of 100 mA cm^{-2} only to reduce the rate at which the bicarbonate reagent concentration decreased with time.) Bicarbonate concentrations were held constant by manually refreshing the 3.0 M $KHCO_3$ electrolyte 500 seconds before each GC measurement. Unlike the catholyte solution, the KOH anolyte solution was not refreshed, since the continuous supply of OH^- from the anion exchange side of the BPM is expected to maintain the pH of the anolyte. The FE_{CO} decreased by merely 3% over this 80 h period for the silver foam electrode. Notably, the composite electrode exhibited a much larger decrease of 16% over the same time period. Moreover, the same electrode used for this 80 h electrolysis experiment could be reused 3 weeks later without any regeneration steps to yield nearly the same performance (Figure S16). These results demonstrate how a free-standing silver foam electrode does not suffer from silver nanoparticle detachment and stability issues common to conventional carbon composite electrodes.

In an industrial setting, the bicarbonate solution feedstock for our electrolyzer could be sourced from a flue gas CO_2 capture system. Consequently, this bicarbonate solution is expected to be contaminated with nitrogen and sulphur containing compounds (SO_4^{2-}, SO_3^{2-}, NH_4^+, NO_3^- etc.) originating from combustion products. We tested the impact of these impurities on the catalytic activity of the foam electrode by electrolysing 3.0 M bicarbonate solutions spiked with 100 ppm of SO_4^{2-}, SO_3^{2-}, NH_4^+, NO_3^-, Cl^- (Figure 6a). The addition of 100 ppm of SO_4^{2-}, SO_3^{2-}, NH_4^+, NO_3^-, Cl^- to the bicarbonate solution had no significant impact on the FE_{CO} or FE_{H2}. However, we found that the addition of NO_3^- to the bicarbonate solution decreased the FE_{CO} from 56% to 28%. The total FE also decreased (from 100% to 58%) (Figure 6a). When the NO_3^- concentration was increased from 100 to 500 ppm, no CO or H_2 was formed from the electrolyzer (i.e., the FE_{CO} and FE_{H2} decreased to 0%) (Figure 5b). This result is

due to the more thermodynamically-favourable NO_3^- reduction outcompeting the CO2RR and HER.[45] This assertion is proved by the restored cell performance observed after switching to a fresh $KHCO_3$ solution, which shows the negligible long-term impact of NO_3^- on the silver foam electrode (Figure 6b). We also found that the *i*-CO_2 generation is independent of NO_3^- concentration. These results collectively show that our bicarbonate electrolyzer has a higher tolerance towards impurities than gaseous CO_2-fed CO2RR electrolyzers which suffer from electrolyzer failure upon addition of flue gas contaminants into the CO_2 feed.[10]

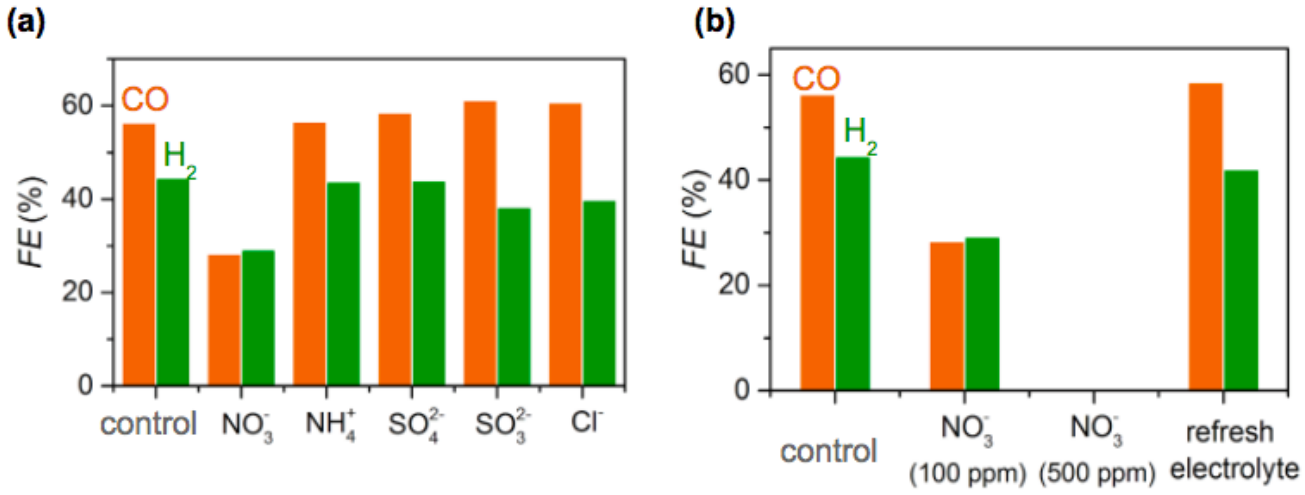

Figure 6. **The impact of flue gas impurities on bicarbonate electrolysis performance**. (a) FE_{CO} and FE_{H2} in the 3.0 M $KHCO_3$ solutions containing 100 ppm impurities. (b) FE of CO and H_2 decreases with the increase of NO_3^- concentration, but the effect is reversible. All electrochemical tests were performed at a constant applied current density of 100 mA cm^{-2} with the silver foam electrode

Conclusion

A key outcome of this study is that we show that aqueous bicarbonate can be electrolyzed into a single carbon-based product with the faradaic efficiencies of 95% at 100 mA cm^{-2} and 55% at 400 mA cm^{-2}. These values are higher than any known CO_2 electrolyzer that uses an aqueous feedstock saturated with CO_2, and are nearly commensurate with electrolyzers that rely on gaseous CO_2 feedstocks. We were

able to achieve these performance metrics by using a free-standing metallic cathodic electrode, which we found to be more effective for electrolyzing liquid bicarbonate solutions than the carbon composite electrode widely used for CO_2RR electrolysis. The electrolytic performance of this foam can be improved with an acid etching process, operation at higher pressure and temperatures, and also by optimizing flow pattern geometries. Importantly, the free-standing electrodes are also far more stable than the conventional GDEs that suffer from catalyst detachment, and the system is generally effective when exposed to common impurities. The free-standing electrodes are also easier to work with when assembling the electrolyzer, and they can be re-used without further regeneration steps. We therefore contend that this architecture provides a viable path for making CO_2 electrolysis compatible with carbon capture schemes.

Author contributions

C.P.B. supervised the project. Z.Z and E.L. conceived the study and Z.Z, E.L, F.H., D.S., generated the figures. Z.Z. and E.L. designed experiments. Z.Z., S.R., G.S. and D.W. performed experiments. D.W. designed the instrumentation for the pressurized experiments. All authors contributed to the final manuscript writing.

Acknowledgements

The authors would like to thank Dr. Tengfei Li and Arthur G. Fink for valuable discussions, David J. Dvorak for performing scanning electron microscopy (SEM) imaging. The authors are grateful to Natural Resources Canada (EIP2-MAT-001), the Canadian Natural Science and Engineering Research Council (RGPIN 337345-13), Canadian Foundation for Innovation (229288), Canadian Institute for Advanced Research (BSE-BERL-162173), TOTAL American Services, Inc (an affiliate of TOTAL SA, France), and the Canada Research Chairs for financial support. This research was undertaken thanks in part to funding from the Canada First Research Excellence Fund, Quantum Materials and Future

Technologies Program. SEM imaging was performed in the Centre for High-Throughput Phenogenomics at the University of British Columbia, a facility supported by the Canada Foundation for Innovation, British Columbia Knowledge Development Foundation, and the UBC Faculty of Dentistry.

Supporting Information:

Experimental methods, electrochemical surface area (ECSA) measurements and Faradaic efficiency calculation, liquid product detection, diagram of the experimental setup, SEM images of the silver foam cathodes, XRD of the silver foam cathodes, cell voltage profile, CO_2 and in-situ generated CO_2 flow rates, ^{1}H-NMR spectra for electrolytes, SEM images before and after 80 h electrolysis of the silver foam electrodes, and silver foam electrode recycle experimental data are included in the Supporting Information.

References

1 D. W. Keith, G. Holmes, D. St. Angelo and K. Heidel, *Joule*, 2018, **2**, 1573–1594.
2 D. M. Weekes, D. A. Salvatore, A. Reyes, A. Huang and C. P. Berlinguette, *Acc. Chem. Res.*, 2018, **51**, 910–918.
3 D. A. Salvatore, D. M. Weekes, J. He, K. E. Dettelbach, Y. C. Li, T. E. Mallouk and C. P. Berlinguette, *ACS Energy Lett.*, 2018, **3**, 149–154.
4 S. Nitopi, E. Bertheussen, S. B. Scott, X. Liu, A. K. Engstfeld, S. Horch, B. Seger, I. E. L. Stephens, K. Chan, C. Hahn, J. K. Nørskov, T. F. Jaramillo and I. Chorkendorff, *Chem. Rev.*, 2019, **119**, 7610–7672.
5 T. Burdyny and W. A. Smith, *Energy & Environmental Science*, 2019, **12**, 1442–1453.
6 A. J. Welch, E. Dunn, J. S. DuChene and H. A. Atwater, *ACS Energy Letters*, 2020, **5**, 940–945.
7 D. Gao, R. M. Arán-Ais, H. S. Jeon and B. R. Cuenya, *Nature Catalysis*, 2019, **2**, 198–210.
8 W. A. Smith, T. Burdyny, D. A. Vermaas and H. Geerlings, *Joule*, 2019, **3**, 1822–1834.
9 B. H. Ko, B. Hasa, H. Shin, E. Jeng, S. Overa, W. Chen and F. Jiao, *Nat. Commun.*, 2020, **11**, 5856.
10 W. Luc, B. H. Ko, S. Kattel, S. Li, D. Su, J. G. Chen and F. Jiao, *J. Am. Chem. Soc.*, 2019, **141**, 9902–9909.
11 A. Stein, T. R. Todd and B. N. Perry, *Appl. Opt.*, 1983, **22**, 3378.
12 G.-M. Lin and C.-S. Chyang, *Energy Fuels*, 2017, **31**, 12417–12424.
13 J. W. Butler, C. Jim Lim and J. R. Grace, *Chemical Engineering Research and Design*, 2011, **89**, 1794–1804.
14 S. Lin, T. Kiga, Y. Wang and K. Nakayama, *Energy Procedia*, 2011, **4**, 356–361.
15 T. Li, E. W. Lees, M. Goldman, D. A. Salvatore, D. M. Weekes and C. P. Berlinguette, *Joule*, 2019, **3**, 1487–1497.
16 Y. C. Li, G. Lee, T. Yuan, Y. Wang, D.-H. Nam, Z. Wang, F. P. García de Arquer, Y. Lum, C.-T. Dinh, O. Voznyy and E. H. Sargent, *ACS Energy Lett.*, 2019, **4**, 1427–1431.
17 D. A. Vermaas and W. A. Smith, *ACS Energy Lett.*, 2016, **1**, 1143–1148.
18 J. Li, G. Chen, Y. Zhu, Z. Liang, A. Pei, C.-L. Wu, H. Wang, H. R. Lee, K. Liu, S. Chu and Y. Cui, *Nature Catalysis*, 2018, **1**, 592–600.
19 A. Z. Weber and J. Newman, *J. Electrochem. Soc.*, 2005, **152**, A677–A688.
20 S. S. Kumar and V. Himabindu, *Materials Science for Energy Technologies*.
21 A. C. de B. V. Dias and Others, Doctor's degree, University of Porto , 2010.
22 C. Xiang, K. M. Papadantonakis and N. S. Lewis, *Materials Horizons*, 2016, **3**, 169–173.
23 K. Zeng and D. Zhang, *Progress in Energy and Combustion Science*, 2010, **36**, 307–326.
24 F. Franco, J. Prior, S. Velizarov and A. Mendes, *NATO Adv. Sci. Inst. Ser. E Appl. Sci.*, 2019, **9**, 284.
25 S. E. S. C. B. E. Achieved, *Platin. Met. Rev.*, 1985, **29**, 98–106.
26 E. W. Lees, M. Goldman, A. G. Fink, D. J. Dvorak, D. A. Salvatore, Z. Zhang, N. W. X. Loo and C. P. Berlinguette, *ACS Energy Letters*, 2020, 2165–2173.
27 G. O. Larrazábal, P. Strøm-Hansen, J. P. Heli, K. Zeiter, K. T. Therkildsen, I. Chorkendorff and B. Seger, *ACS Appl. Mater. Interfaces*, 2019, **11**, 41281–41288.
28 R. T. J. Porter, M. Fairweather, M. Pourkashanian and R. M. Woolley, *Int. J. Greenhouse Gas Control*, 2015, **36**, 161–174.
29 S. Ren, D. Joulié, D. Salvatore, K. Torbensen, M. Wang, M. Robert and C. P. Berlinguette, *Science*, 2019, **365**, 367–369.
30 A. Dutta, C. E. Morstein, M. Rahaman, A. Cedeño López and P. Broekmann, *ACS Catal.*, 2018, **8**, 8357–8368.
31 T. Kottakkat, K. Klingan, S. Jiang, Z. P. Jovanov, V. H. Davies, G. A. M. El-Nagar, H. Dau and C. Roth, *ACS Appl. Mater. Interfaces*, 2019, **11**, 14734–14744.
32 Q. Lu, J. Rosen, Y. Zhou, G. S. Hutchings, Y. C. Kimmel, J. G. Chen and F. Jiao, *Nat. Commun.*, 2014, **5**, 3242.
33 L.-C. Weng, A. T. Bell and A. Z. Weber, *Physical Chemistry Chemical Physics*, 2018, **20**, 16973–16984.
34 B. Kim, F. Hillman, M. Ariyoshi, S. Fujikawa and P. J. A. Kenis, *J. Power Sources*, 2016, **312**, 192–198.

35 Y. Feng, H. Zheng, Z. Zhu and F. Zu, *Mater. Chem. Phys.*, 2003, **78**, 196–201.
36 M. S. Ismail, T. Damjanovic, D. B. Ingham, M. Pourkashanian and A. Westwood, *J. Power Sources*, 2010, **195**, 2700–2708.
37 R. Omrani and B. Shabani, *Int. J. Hydrogen Energy*, 2017, **42**, 28515–28536.
38 N. Kampman, M. Bickle, M. Wigley and B. Dubacq, *Chem. Geol.*, 2014, **369**, 22–50.
39 K. S. Johnson, *Limnol. Oceanogr.*, 1982, **27**, 849–855.
40 Z. Zhang, L. Melo, R. P. Jansonius, F. Habibzadeh, E. R. Grant and C. P. Berlinguette, *ACS Energy Lett.*, 2020, **5**, 3101–3107.
41 P. Lobaccaro, M. R. Singh, E. L. Clark, Y. Kwon, A. T. Bell and J. W. Ager, *Phys. Chem. Chem. Phys.*, 2016, **18**, 26777–26785.
42 D. A. Vermaas, S. Wiegman, T. Nagaki and W. A. Smith, *Sustainable Energy & Fuels*, 2018, **2**, 2006–2015.
43 D. G. Wheeler, B. A. W. Mowbray, A. Reyes, F. Habibzadeh, J. He and C. P. Berlinguette, *Energy Environ. Sci.*
44 B. De Mot, M. Ramdin, J. Hereijgers, T. J. H. Vlugt and T. Breugelmans, *ChemElectroChem*, 2020, **7**, 3839–3843.
45 Y. Wang, A. Xu, Z. Wang, L. Huang, J. Li, F. Li, J. Wicks, M. Luo, D.-H. Nam, C.-S. Tan, Y. Ding, J. Wu, Y. Lum, C.-T. Dinh, D. Sinton, G. Zheng and E. H. Sargent, *J. Am. Chem. Soc.*, 2020, **142**, 5702–5708.